ISSN 1067-8212, Russian Journal of Non-Ferrous Metals, 2020, Vol. 61, No. 5, pp. 583–591. © Allerton Press, Inc., 2020.
Russian Text © The Author(s), 2020, published in Izvestiya Vysshikh Uchebnykh Zavedenii, Poroshkovaya Metallurgiya i Funktsional'nye Pokrytiya, 2020, No. 1, pp. 65–74.

NANOSTRUCTURED MATERIALS AND FUNCTIONAL COATINGS

Nanoscale Nickel-Containing Powders for Use in CO and NO_2 Gas Sensors

M. V. Kuznetsov[a], *, A. V. Safonov[a], **, D. A. Bobreshov[a], *, O. V. Belousova[b], ****, and Iu. G. Morozov[b], *******

[a]*All-Russian Research Institute for Problems of Civil Defense and Emergencies, Ministry of Emergency Situations, Moscow, 121352 Russia*

[b]*Merzhanov Institute of Structural Macrokinetics and Materials Science, Russian Academy of Sciences, Chernogolovka, Moscow oblast, 142432 Russia*

**e-mail: maxim1968@mail.ru*

***e-mail: safa2004@mail.ru*

****e-mail: bobreshovdenis@yandex.ru*

*****e-mail: belous@ism.ac.ru*

******e-mail: morozov@ism.ac.ru*

Received November 22, 2019; accepted December 30, 2019

Abstract—This paper investigates the physicochemical characteristics and gas-sensitivity mechanisms of nickel oxide (NiO) and nickel ferrite ($NiFe_2O_4$) obtained by levitation-jet synthesis LJS). Properties of synthesized materials were examined using various spectroscopic methods. XPS showed that the presence of Ni^{3+} ions in samples reduced significantly with an increase in the specific surface area of the powders and a decrease in the average diameter of their particles. In this regard, it can be concluded that the number of uncompensated Ni^{2+} vacancies in such samples also decreases and the concentration of O^{2-} vacancies, on the contrary, increases significantly. The Raman spectra of nanoscale NiO lacked a magnon band, which is usually observed at $\nu = 1500$ cm^{-1}, whereas the spectrum of nanoferrite sample had a pronounced 2M band, which indicates an increase in spin correlation. According to the analysis of UV spectra of the samples, there is an increase in reflectivity values with an increase in wavelength for large nanoparticles when compared to the corresponding values for small particles. In this regard, we suggested that Ni-based oxide nanoparticles are semiconductors with an indirect transition to band-gap energy, and this is in sharp contrast to the data obtained earlier by other researchers. The gas sensitivity of nanoscale powders was investigated in relation to carbon monoxide and nitrogen dioxide at operating temperatures of 350–500°C. An evaluation of the results made it possible to conclude that the operating characteristics of the sensors that we propose are superior in a number of parameters to the similar characteristics of sensors made of commercial powders, as well as of powders obtained by other synthetic methods.

Keywords: levitation-jet synthesis, nanoparticles, nickel oxide, nickel ferrite, gas-sensing properties, gas sensors, carbon monoxide, nitrogen dioxide

DOI: 10.3103/S1067821220050089

INTRODUCTION

In recent decades, gas sensors created based on metal oxide semiconductors (MOS) using various laboratory or industrial technologies have been the subject of intensive research with a view to their possible application for monitoring and controlling production processes, as well as for assessing the quality of the environment [1]. Moreover, such sensors have been used in many technological processes, including those with commercial applications [2]. However, there is a certain limitation associated with their low selectivity to the effects of gases when using sensors that are bulky structures [3]. Their selectivity can be improved through various methods, including precision temperature control and the use of certain surface additives [4]. One of the most effective methods in this direction is the use of nanopowders as working materials [5].

Relatively recently, nickel oxide (NiO), as well as ferrites (such as $NiFe_2O_4$), have been used as materials for gas-sensitive sensors for detecting potentially hazardous gases of various types [6–8]. Recently, when conducting research into nanoscale magnetic structures, much attention has been paid to the controlled

Table 1. Synthesis conditions and some physicochemical characteristics of nickel-containing nanoparticles obtained by the LJS method

Sample	Synthesis conditions	d, nm	NiO, vol %	E_g, eV	S_{spec}, m^2/g
N1	500 L/h He; 1 g/h Ni	23	17	2.22	29.8
N2	1000 L/h He; 200 L/h O_2; 1 g/h	8	100	2.72	103.0
N3	1000 L/h He; 100 L/h O_2; 0.4 g/h	7	100	3.28	117.0
N4	NiO (TU 6-09-5095-83)	230	100	3.18	3.77
N5	NiO (Aldrich 6-67)	37 μm	100	1.50	23.6
N6	500 L/h He; 9 L/h of air; 2 g/h Ni; 3.5 g/h Fe	31	0	–	36.3

synthesis of nanosized ferrites, since the distribution of cations and the resulting magnetic properties of powders differ significantly in comparison with their bulky counterparts [5, 9].

For the synthesis of nanosized powders of spinel nickel ferrite ($NiFe_2O_4$), the following techniques were developed: coprecipitation [10], the sol–gel method [11], shock-wave synthesis [12], mechanical alloying [13], etc. However, until now no alternative, relatively simple methods have been developed for the synthesis of nanocrystalline $NiFe_2O_4$, which is currently obtained as a result of rather complex multistage synthetic approaches. Among these methods, levitation-jet synthesis (LJS) has real advantages, since it allows the simultaneous control of the size, shape, and oxidation state of synthesized nanoparticles [14].

The aim of this work is to synthesize Ni/NiO and $NiFe_2O_4$ nanopowders by LJS; investigate the morphology, phase composition, and optical–spectroscopic characteristics of the nanoparticles; and fabricate gas sensors based on these nanoparticles and examine their gas sensitivity in the presence of trace concentrations of carbon monoxide and nitrogen dioxide.

EXPERIMENTAL PART

Materials, Equipment, and Research Methods

Synthesis of nanomaterials. Nickel-containing oxide nanoparticles were synthesized using the modified Gen–Miller levitation-jet method [15–18]. In this method, a droplet of metal (alloy) is suspended inside a quartz tube of a certain size and is heated to its melting point and initial vaporization by means of an electromagnetic field generated by a high-frequency generator. The levitating droplet is blown with a controlled flow of an inert He/Ar gas at normal pressure. For the formation and evaporation of the levitating droplet, wires of pure metals are used which continuously supply metal to the high-temperature reaction zone. For the synthesis of oxide nanoparticles, the required amount of gaseous oxygen/air was introduced into the main gas flow.

Methods for investigating the synthesized materials. The crystal structure and phase composition of the corresponding nanopowders were studied by X-ray diffraction using the DRON-3M diffractometer (CuK_α or FeK_α-radiation) manufactured by NPP Burevestnik (St. Petersburg). X-ray phase analysis (XPA) was carried out using the Crystallographica SearchMatch and PowderCell software and the PDF2 database. The morphology of the powders was studied by transmission electron microscopy (TEM) using a JEM-1200 EX II microscope (Jeol, Japan) and scanning electron microscopy (SEM) using a LEO 1450 microscope (Carl Zeiss, Germany). The electron micrographs were analyzed in the AxioVision imaging software in order to determine the average particle size. The specific surface of the nanoparticles was studied by the four-point BET method using the SORBI-M device (ZAO META, Novosibirsk). X-ray photoelectron spectra (XPS) were obtained using the Thermo Scientific X-ray Photoelectron Spectrometer (United States) with the monochrome AlK_α source (1486.6 eV). UV spectra in the visible range were detected using the Lambda 950 spectrocolorimeter (PerkinElmer Inc., United States) with a built-in spherical detector. Raman spectra were detected at room temperature using the InVia Raman tool manufactured by Renishaw.

Fabrication of gas sensors. The resulting nanopowders were mixed with a special composition for preparing a suspension in accordance with the previously developed technique [19]. These suspensions were applied directly to golden electrodes located on the surfaces of alundum plates 3 × 3 mm in size by screen printing. Then they were calcined in a furnace at t = 600°C for 1 h [20, 21]. Experiments for determining the gas sensitivity were carried out using the setup described earlier [20] at the constant operating temperature in the range t = 300–500°C. Responses of the sensors to the action of a number of gases, namely carbon monoxide and nitrogen dioxide, in ecologically significant concentrations were investigated [1]. Specific characteristics of the materials of the gas sensors created based on synthesized nanopowders are given in Table 1.

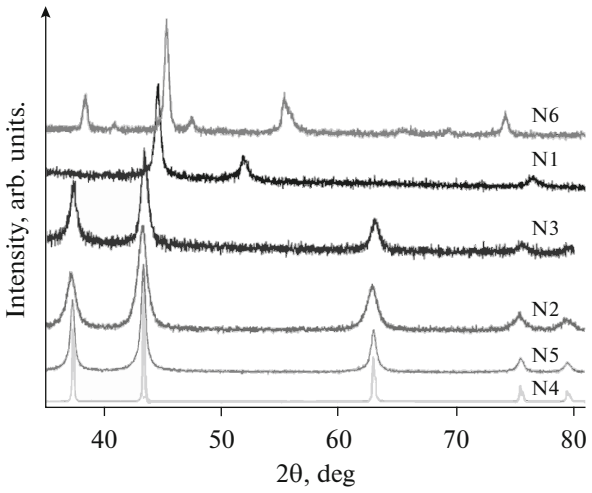

Fig. 1. X-ray spectra of nanopowder samples obtained in the LJS mode. Sample numbers correspond to the nomenclature presented in Table 1.

RESULTS AND DISCUSSION

XPA Results

Figure 1 shows X-ray diffraction patterns of samples N1–N6. For sample N1, the phase of cubic nickel (JCPDS card 04-0850) was determined as the principal phase with parameter $a = 0.3524$ nm. Diffraction patterns of samples N2–N5 confirm that these samples contain pure rhombohedral NiO (JCPDS card 44-1159) as the principal phase with unit-cell parameters $a = 0.2955$ nm and $c = 0.7228$ nm. No other impurity phases were found in the samples. The powder diffraction pattern of sample N6 corresponded to the structure of nickel nanoferrite $NiFe_2O_4$ (JCPDS 44-1485) with a spinel structure and $a = 0.8339$ nm [22].

Results of Electron Microscopy and Examination of the Specific Surface Area of Powders

Micrographs of nanoparticles of the nickel-containing powders obtained using transmission and scanning electron microscopes (Fig. 2) confirmed the cubic morphology with an average particle size $d <$ 100 nm in all Ni/NiO samples. The exception was commercial material N6, the powder particles of which had an oval shape and $d > 10$ μm. The morphology of the $NiFe_2O_4$ (N6) sample (Fig. 2f) differs significantly from that in N1–N5. The particle shape in N6 was predominantly hexagonal. Specific surface areas (S_{spec}) for the investigated powders are given in Table 1.

Results of Powder Studies Using XPS Spectroscopy

Various practically important physical properties of Ni-based nanoparticles arise due to the dominant contribution to their defect structure made by cations (Ni^{2+}) and anions (O^{2-}), which are the main sources of defects in NiO [23]. The presence of each of the

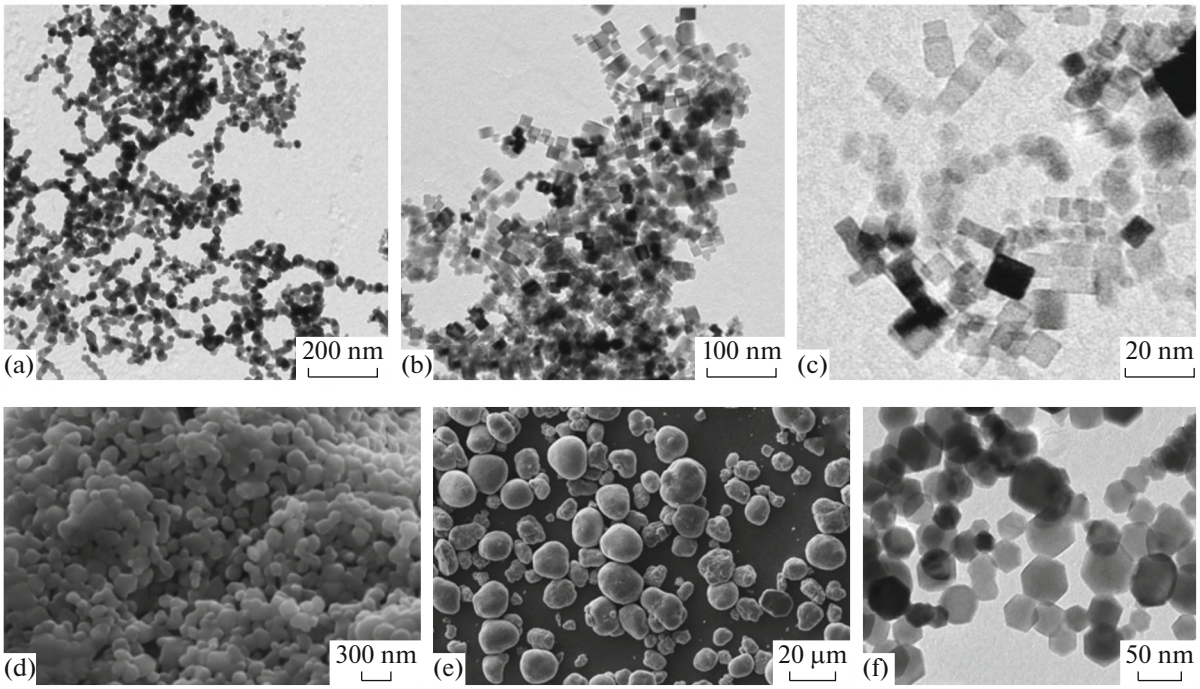

Fig. 2. Micrographs of nanopowder samples obtained using transmission and scanning electron microscopy: (a) N1, (b) N2, (c) N3, (d) N4, (e) N5, and (f) N6. Sample numbers and synthesis parameters are given in Table 1.

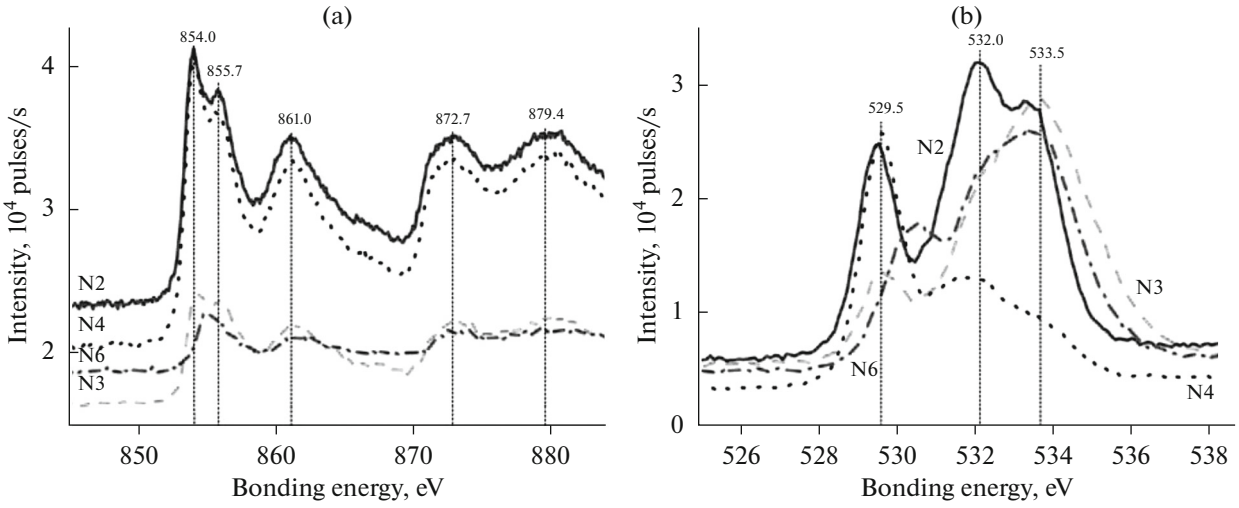

Fig. 3. XPS of Ni 2*p* (a) and O 1*s* (b) of the studied Ni-containing nanopowders.

Ni^{2+} vacancies in their structure leads to the transformation of two neighboring Ni^{2+} ions into Ni^{3+} ions to ensure charge neutrality, thereby causing lattice distortion. The presence of Ni^{3+} ions in the samples was confirmed using XPS, the results of which are shown in Fig. 3. Two pronounced peaks at U = 854.0 and 872.7 eV in the spectrum of Ni 2*p* correspond to the doublet of Ni $2p_{3/2}$ and Ni $2p_{1/2}$ (see Fig. 3a).

As a result of stirring processes in the samples, their spectra also contain peaks at U = 879.4 and 861.0 eV [24]. In the O 1*s* spectra (Fig. 3b) of sample N2, the peaks at U = 529.5 and 532.0 eV indicate that its structure contains O^{2-} ions bound to Ni^{2+} and Ni^{3+}, respectively. For sample N3, the corresponding peaks were detected at U = 529.7 and 533.5 eV, respectively. After comparing the intensities of the corresponding peaks in these two samples, it became clear that the presence of Ni^{3+} in sample N3 decreased significantly [23]. Thus, it can be concluded that sample N3, when compared to N2, had fewer uncompensated Ni^{2+} vacancies and a significantly higher concentration of O^{2-} vacancies, like in the ferrite sample (N6).

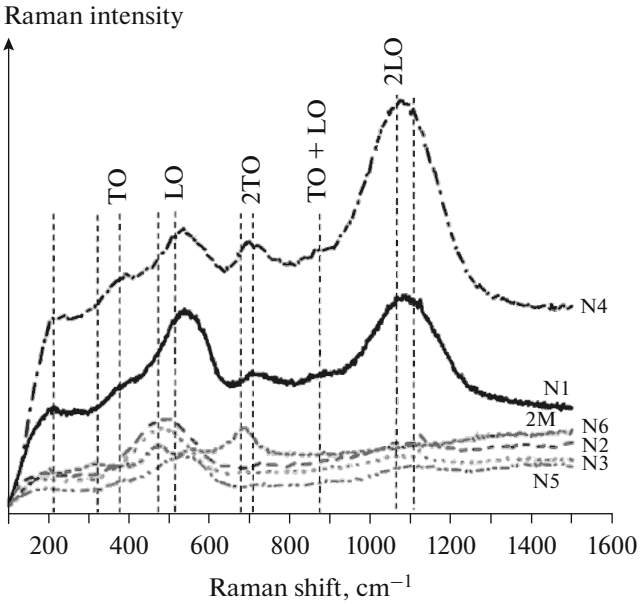

Fig. 4. Raman spectra of powders of nanosized materials obtained by the LJS method.

Results of Investigating the Powders Using Raman Spectroscopy

Raman spectroscopy (RS) is very sensitive to the state of the microstructure of nanocrystalline materials. The Raman spectrum of pure NiO obtained at room temperature consists of several bands: five vibrational bands of the one-phonon (1P) mode TO (at ~400–440 cm^{-1}) and LO (at ~560 cm^{-1}); two-phonon (2P) modes 2TO (at ~740 cm^{-1}), TO + LO (at ~925 cm^{-1}), and 2LO (at ~1100 cm^{-1}); and two-magnon (2M) band at ~1500 cm^{-1} [25]. Most of the spectra of the NiO samples (Fig. 4) demonstrate the presence of Raman bands located at 380, 520, 710, 880, and 1080 cm^{-1}, respectively. These shifts in the spectra correspond to the structure of nanosized NiO [26]. It was noted that the intensities of two Raman bands (520 and 1080 cm^{-1}) increase with an increase in the average size of nanoparticles. The Raman spectrum of our samples lacked the magnon band, which is usually observed at 1500 cm^{-1}. However, the study of the spectrum of the ferrite image (N6) showed the presence of a pronounced 2M band, while other bands were less pronounced.

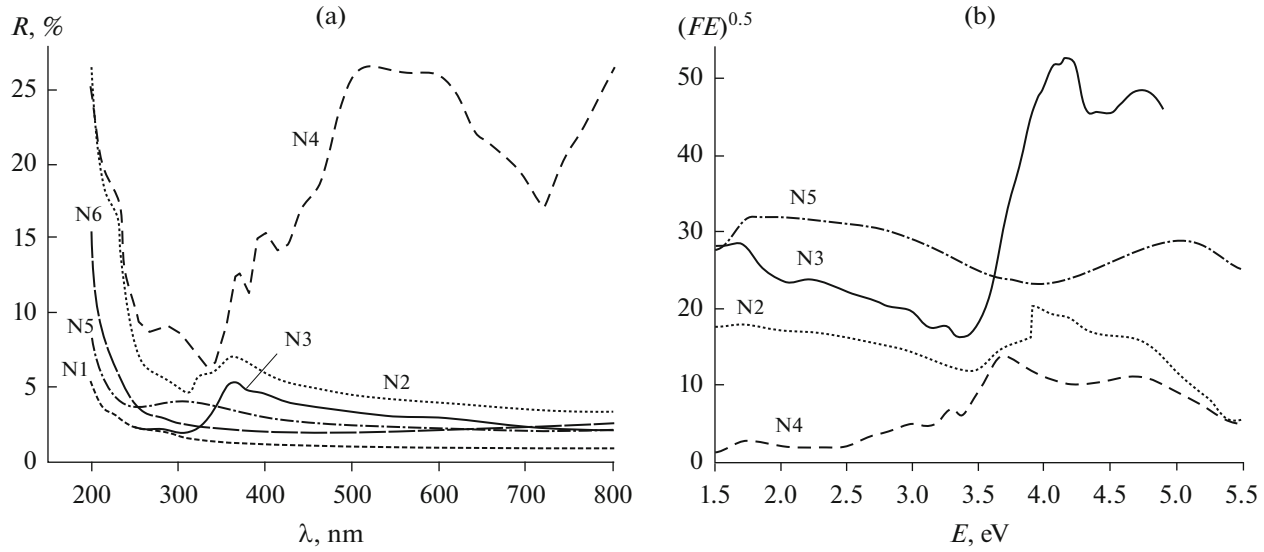

Fig. 5. UV diffuse reflectance spectra in the visible region (a) and the values of the band gap in the spectra of a number of nanoparticles determined using function (1) (b).

Results of Investigating the Powders Using Ultraviolet–Visible Spectroscopy

The diffuse reflectance UV spectra for some samples are shown in Fig. 5a. An analysis of Fig. 5a showed that large nanoparticles exhibit higher reflectance values with the increasing wavelength when compared with the corresponding values for small particles, which is a consequence of the scattered radiation of clusters of NiO nanoparticles. All spectra were analyzed using the Kubelka–Munk function $F(R)$ [27] associated with diffuse reflection by the following expression:

$$F = (1 - R)^2/(2R). \quad (1)$$

Here, R is the absolute reflectance and F is the coefficient equivalent to the absorption coefficient. The most effective approach to the analysis of such spectra is to determine the transition band for the gap E_g, which was estimated by plotting $(FE)^{0.5}$ as a function of the photon energy E (Fig. 5b) [28]. The linear parts of the corresponding curves were extrapolated to zero in order to determine the value of the band gap [29].

Investigation into the Gas Sensitivity of Sensors Based on Nickel-Containing Powders

In this work, the gas-sensitive properties of the sensors based on NiO and $NiFe_2O_4$ nanopowders obtained by LJS were investigated. In addition, the results were compared with the gas sensitivity of the sensors based on commercial NiO powders. The sensors were tested under conditions of exposure to various concentrations of gases at specific operating temperatures in order to identify optimal experimental conditions for each specific device.

It is known that MOS sensors are mainly evaluated in terms of their maximum sensitivity when exposed to the test gas and heated to temperatures usually in the range of 200–500°C [30]. It is generally accepted that changes in the electrical resistance of the sensor happen either due to the presence of space charge, effects, and surface vibrations caused by ionosorbed gaseous impurities or due to alterations in the oxygen stoichiometry of the used gas-sensitive material [31]. Typically, n-type semiconductor materials react to the presence of a reducing gas in the atmosphere by the decreasing sensor resistance and, accordingly, the increasing electrical resistance R/R_0 when an oxidizing gas is supplied [3]. The p-type semiconductor materials exhibit the opposite behavior. NiO is a p-type semiconductor material and is widely used as a working material for sensors of various gases. The presence of satisfactory gas-sensitive characteristics of spinel ferrite ($NiFe_2O_4$) was also confirmed in the studies of other authors [32]. Usually it is a p-type semiconductor, whose behavior is determined by the presence of holes between Ni^{2+} and Ni^{3+} in the octahedral sites of the corresponding lattices [33].

In our study, the sensor based on commercial NiO powders, as well as the sensors made using NiO nanopowders produced by LJS, demonstrated the presence of p-type conductivity, while the sensor based on nickel ferrite ($NiFe_2O_4$) was characterized by n-type conductivity; therefore, its response was identified as R_0/R.

Behavior of gas sensors in the presence of carbon monoxide. The fabricated sensors were investigated in the presence of carbon monoxide in concentrations from 50 to 500 ppm, as well as at various temperatures (in the range of 300–500°C). The sensors showed neg-

Table 2. Responses of sensors based on materials produced by LJS to temperature (t) and concentration (c) of carbon monoxide

t, °C	c, ppm	R/R_0 (R_0/R)					
		N1	N2	N3	N4	N5	N6
300	50	0.021	0.029	0.016	0.024	0.031	0
	100	0.034	0.043	0.031	0.034	0.052	0
	200	0.043	0.057	0.034	0.041	0.063	0
	300	0.05	0.065	0.035	0.045	0.075	0
	500	0.057	0.072	0.035	0.046	0.087	0
350	50	0.077	0.144	0.044	0.087	0.107	0
	100	0.033	0.064	0.006	0.035	0.081	0.008
	200	0.037	0.065	0.002	0.031	0.103	0
	300	0.044	0.073	0	0.03	0.121	0.008
	500	0.056	0.081	0.001	0.034	0.143	0.033
400	50	0.092	0.141	0.089	0.103	0.107	0
	100	0.054	0.079	0.041	0.053	0.107	0
	200	0.065	0.099	0.039	0.055	0.142	0.003
	300	0.078	0.114	0.042	0.06	0.165	0.014
	500	0.095	0.127	0.042	0.067	0.195	0.032
450	50	0.05	0.068	0.066	0.054	0.055	0.014
	100	0.059	0.089	0.046	0.052	0.093	0.02
	200	0.081	0.102	0.054	0.063	0.128	0.033
	300	0.096	0.117	0.054	0.073	0.154	0.033
	500	0.116	0.144	0.057	0.181	0.087	0.042
500	50	0.092	0.127	0.184	0.114	0.049	0
	100	0.062	0.075	0.107	0.061	0.069	0
	200	0.089	0.109	0.115	0.076	0.102	0.006
	300	0.107	0.135	0.123	0.089	0.128	0.01
	500	0.130	0.169	0.127	0.106	0.162	0.008

ligible response to these test concentrations in the studied temperature range (Table 2). Similar results were obtained in [34], when the CO concentration of <500 ppm was applied to a gas sensor based on $NiFe_2O_4$. The sensor response values slightly increased during experiments with CO concentrations exceeding 1000 ppm [34].

Behavior of gas sensors in the presence of nitrogen dioxide. At relatively low concentrations of NO_2 (at the ppb level), the behavior of the sensors was as follows: in n-type sensors, in the presence of NO_2, the electrical resistance increased, and electrical resistance decreased in the sensors originally characterized as p-type.

The sensors generally showed a rather weak response to the presence of NO_2, except for a sensor based on nickel ferrite (Fig. 6). The latter, at t = 350°C, began to show a response in the presence of NO_2 at a concentration of 50 ppb; this response significantly increased with the temperature decreasing to 300°C. When gas was supplied at a concentration of 500 ppb, the peak maximum in the sensor response graph decreased, which could be due to a number of near-surface exchange reactions.

We would like to note the increase in the response level of the N6 sensor based on nickel ferrite to the presence of NO_2 at a concentration of 500 ppb in the atmosphere by more than an order of magnitude in comparison with similar indicators of sensors based on commercial nickel oxide. The increase in the response level was also significant in comparison with other sensors based on NiO nanoparticles obtained in the LJS mode.

Similar studies by other authors reported the gas sensitivity of NiO-based nanoparticles to NO_2. They found similar effects, confirming that these materials were weakly sensitive to the presence of NO_2 in the atmosphere, even at concentrations about 10 ppm [35, 36]. Thus, our gas sensor based on nickel ferrite powder demonstrated high stability of operation when exposed to insignificant concentrations of the studied gases, which indicates good prospects for its use in terms of selectivity.

It should also be noted that the gas sensitivity of the sensor based on nickel ferrite obtained in the LJS mode was much better than that of other sensors based on nanoparticles obtained in the LJS mode (NiO) prepared in this study, as well as with respect to the characteristics of the sensor created using commercial NiO powders. The N1 and N2 sensors are also promising for testing in various gas atmospheres. It is interesting to note that, although the N2 and N3 sensors have similar microstructures and particle morphology, they respond differently to the presence of the gases of interest. This may be a result of certain differences in the conditions of the LJ synthesis and/or the result of

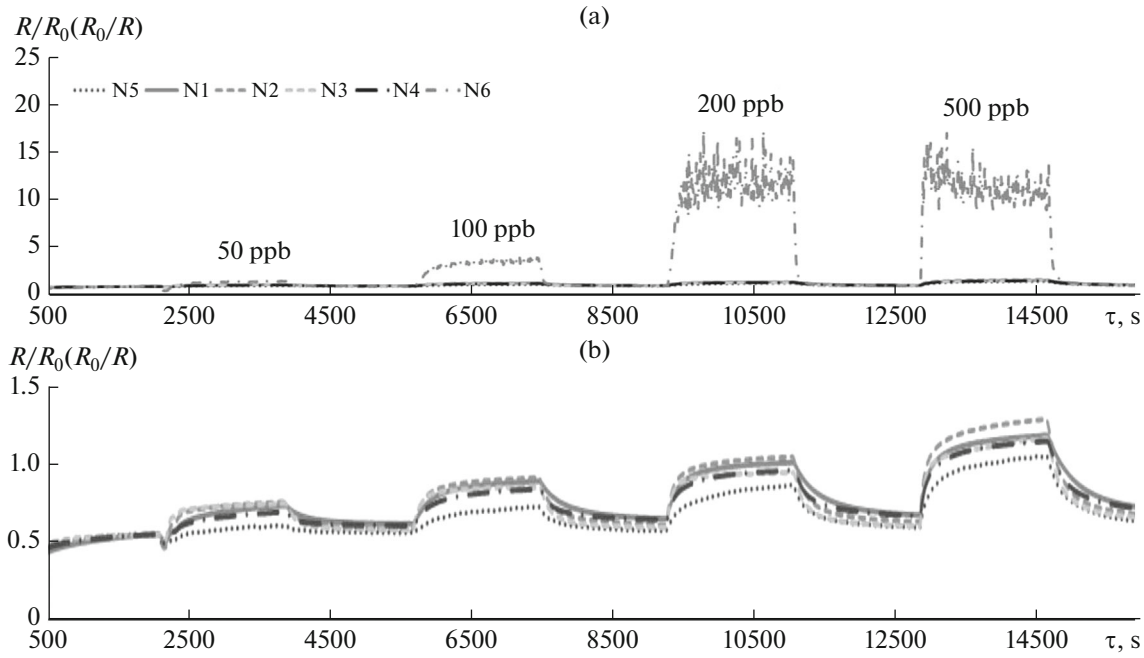

Fig. 6. Responses of N1–N6 sensors to the presence of nitrogen dioxide in the atmosphere in various concentrations (50–500 ppb) at the operating temperature of 300°C (a) and its exploded view for responses of sensors N1–N5 (b).

the effect of materials sintering as early as at the stages of the direct fabrication of the sensor. It is possible that this also affected the microstructure of gas-sensitive materials in such a way that the access of gases through the near-surface layers was somewhat limited (for example, for the N3 sensor).

CONCLUSIONS

For the controlled (in terms of the morphology and sizes of nanoparticles) synthesis of nanopowders of metal oxides based on nickel (including a complex oxide material such as spinel nickel ferrite), in order to assess the possibility of their use as a basis for creating gas-sensitive sensors, the method of LJS was employed. Materials synthesized in the LJS mode and sensors based on them, in comparison with sensors created on the basis of commercial material (NiO), demonstrate higher performance. A gas sensor based on $NiFe_2O_4$ showed the strongest response to the presence of the gases under study, including at extremely low concentrations, despite the presence of other sensors in the block with it, which had even more developed surfaces of working materials. Moreover, this sensor showed varying degrees of sensitivity with respect to the gases under investigation, thus indicating a high potential in terms of selectivity. Thus, it is confirmed that the LJS method is promising for the production of simple and complex oxide materials, simultaneously allowing for precise control over size, shape, and composition of nanoparticles, which, in turn, makes it possible to increase the productivity of gas sensors created on the basis of LJS materials. Sensors of this type are promising for future environmental and commercial applications involving the continuous analysis of the composition, quality, and pollution of ambient air, even in cases of their long-term operation.

CONFLICT OF INTEREST

The authors declare that they have no conflicts of interest.

REFERENCES

1. Rumyantseva, M.N., Kovalenko, V.V., Gas'kov, A.M., and Pagnier, T., Metal-oxide based nanocomposites as materials for gas sensors, *Russ. J. Gen. Chem.,* 2008, vol. 78, no. 5, pp. 1081–1092. https://doi.org/10.1134/S1070363208050411
2. Dey, A., Semiconductor metal oxide gas sensors: A review, *Mater. Sci. Eng., B,* 2018, vol. 229, pp. 206–217. https://doi.org/10.1016/j.mseb.2017.12.036
3. Williams, D.E., Semiconducting oxides as gas-sensitive resistors, *Sens. Actuators, B,* 1999, vol. 57, nos. 1–3, pp. 1–16. https://doi.org/10.1016/S0925-4005(99)00133-1
4. Binions, R., Afonja, A., Dungey, S., Lewis, D.E., Parkin, I.P., and Williams, D.E., Discrimination effects in zeolite modified metal oxide semiconductor gas sensors, *IEEE Sens. J.,* 2011, vol. 11, no. 5, pp. 1145–1151. https://doi.org/0.1109/JSEN.2010.2084079

5. Lee, P.Y., Ishizaka, K., Suematsu, H., Jiang, W., and Yatsui, K., Magnetic and gas sensing property of nanosized $NiFe_2O_4$ powders synthesized by pulsed wire discharge, *J. Nanopart. Res.,* 2006, vol. 8, no. 1, pp. 29–35. https://doi.org/10.1007/s11051-005-5427-z
6. Ju, D., Xu, H., Xu, Q., Gong, H., Qiu, Z., and Guo, J., High triethylamine-sensing properties of NiO/SnO_2 hollow sphere P-N heterojunction sensors, *Sens. Actuators, B,* 2015, vol. 215, pp. 39–44. https://dx.doi.016/j.snb.2015.03.015.
7. Arshak, K. and Gaidan, I., NiO/Fe_2O_3 polymer thick films as room temperature gas sensors, *Thin Solid Films,* 2006, vol. 495, nos. 1–2, pp. 286–291. https://doi.org/10.1016/j.tsf.2005.08.298
8. Darshane, S.L., Suryavanshi, S.S., and Mulla, I.S., Nanostructured nickel ferrite: A liquid petroleum gas sensor, *Ceram. Int.,* 2009, vol. 35, no. 5, pp. 1793–1797. https://doi.org/10.1016/j.ceramint.2008.10.013
9. Ortega, D., Kuznetsov, M.V., Morozov, Yu.G., Belousova, O.V., and Parkin, I.P., Thermal relaxation and collective dynamics of interacting aerosol-generated hexagonal $NiFe_2O_4$ nanoparticles, *Phys. Chem. Chem. Phys.,* 2013, vol. 15, no. 48, pp. 20830–20838. https://doi.org/10.1039/c3cp53981d
10. Chen, N.-S., Yang, X.-J., Liu, E.-S., and Huang, J.-L., Reducing gas-sensing properties of ferrite compounds MFe_2O_4 (M = Cu, Zn, Cd and Mg), *Sens. Actuators, B,* 2000, vol. 66, no. 1–3, pp. 178–180. https://doi.org/10.1016/S0925-4005(00)00368-3
11. Chen, D.-H. and He, X.-R., Synthesis of nickel ferrite nanoparticles by sol-gel method, *Mater. Res. Bull.,* 2001, vol. 36, nos. 7–8, pp. 1369–1377. https://doi.org/10.1016/S0025-5408(01)00620-1
12. Liu, J., He, H., Jin, X., Hao, Z., and Xu, Z., Synthesis of nanosized nickel ferrites by shock waves and their magnetic properties, *Mater. Res. Bull.,* 2001, vol. 36, nos. 13–14, pp. 2357–2363. https://doi.org/10.1016/S0025-5408(01)00722-X
13. Suematsu, H., Ishizaka, K., Kinemuchi, Y., Suzuki, T., Jiang, W., and Yatsui, K., Novel critical temperature resistor of sintered Ni-Fe-O nanosized powders, *J. Mater. Res.,* 2004, vol. 19, no. 4, pp. 1011–1014. https://doi.org/10.1557/JMR.2004.0131
14. Ortega, D., Kuznetsov, M.V., Morozov, Yu.G., Belousova, O.V., and Parkin, I.P., Thermal relaxation and collective dynamics of interacting aerosol-generated hexagonal $NiFe_2O_4$ nanoparticles, *Phys. Chem. Chem. Phys.,* 2013, vol. 15, no. 48, pp. 20830–20838. https://doi.org/10.1039/c3cp53981d
15. Gen, M.Ya. and Miller, A.V., Levitation method for producing ultrafine metal powders, *Poverkhnost,* 1983, no. 2, pp. 150–154.
16. Kondrat'eva, T.A., Morozov, Y.G., and Chernov, E.A., Effect of conditions of manufacture on the properties of ultrafine nickel powder, *Sov. Powder Metall. Met. Ceram.,* 1987, vol. 26, no. 10, pp. 793–795. https://doi.org/10.1007/BF00794359
17. Krasnov, A.P., Morozov, Y.G., and Chernov, E.A., Characteristic features of the vaporization mechanism in the crucible-free production of aerosol particles, *Powder Technol.,* 1994, vol. 81, no. 1, pp. 93–98. https://doi.org/10.1016/0032-5910(94)02871-0
18. Morozov, Y.G., Belousova, O.V., Kuznetsov, M.V., Ortega, D., and Parkin, I.P., Electric field-assisted levitation-jet aerosol synthesis of Ni/NiO nanoparticles, *J. Mater. Chem.,* 2012, vol. 22, no. 22, pp. 11214–11223. https://doi.org/10.1039/c2jm31233f
19. Binions, R., Davies, H., Afonja, A., Dungey, S., Lewis, D., Williams, D.E., and Parkin, I.P., Zeolite-modified discriminating gas sensors, *J. Electrochem. Soc.,* 2009, vol. 156, no. 3, pp. J46–J51. https://doi.org/10.1149/1.3065436
20. Peveler, W.J., Binions, R., Hailes, S.M.V., and Parkin, I.P., Detection of explosive markers using zeolite modified gas sensors, *J. Mater. Chem. A,* 2013, vol. 1, no. 17, pp. 2613–2620. https://doi.org/10.1039/c2ta01027e
21. Hernández, P.T., Naik, A.J.T., Newton, E.J., Hailes, S.M.V., and Parkin, I.P., Assessing the potential of metal oxide semiconducting gas sensors for illicit drug detection markers, *J. Mater. Chem. A,* 2014, vol. 2, no. 23, pp. 8952–8960. https://doi.org/10.1039/c4ta00357h
22. Costa, A.C.F.M., Lula, R.T., Kiminami, R.H.G.A., Gama, L.F.V., de Jesus, A.A., and Andrade, H.M.C., Preparation of nanostructured $NiFe_2O_4$ catalysts by combustion reaction, *J. Mater. Sci.,* 2006, vol. 41, no. 15, pp. 4871–4875. https://doi.org/10.1007/s10853-006-0048-1
23. Madhu, G. and Biju, V., Nanostructured amorphous nickel oxide with enhanced anti- oxidant activity, *J. Alloys Compd.,* 2015, vol. 637, pp. 62–69. https://doi.org/10.1016/j.jallcom.2015.02.157
24. Biju, V., Ni 2p X-ray photoelectron spectroscopy study of nanostructured nickel oxide, *Mater. Res. Bull.,* 2007, vol. 42, no. 5, pp. 791–796. https://doi.org/10.1016/j.materresbull.2006.10.009
25. Mironova-Ulmane, N., Kuzmin, A., Sildos, I., and Pärs, M., Polarization dependent Raman study of single-crystal nickel oxide, *Cent. Eur. J. Phys.,* 2011, vol. 9, no. 4, pp. 1096–1099. https://doi.org/10.2478/s11534-010-0130-9
26. Tadic, M., Panjan, M., Markovic, D., Stanojevic, B., Jovanovic, D., Milosevic, I., and Spasojevic, V., NiO core-shell nanostructure with ferromagnetic-like behavior at room temperature, *J. Alloys Compd.,* 2014, vol. 586, no. 1, Suppl., pp. S322–S325. https://doi.org/10.1016/j.jallcom.2012.10.166
27. Simmons, E.L., Diffuse reflectance spectroscopy: a comparison of the theories, *Appl. Opt.,* 1975, vol. 14, no. 6, pp. 1380–1386. https://doi.org/10.1364/AO.14.001380
28. Rehman, S., Mumtaz, A., and Hasanain, S.K., Size effects on the magnetic and optical properties of CuO nanoparticles, *J. Nanopart. Res.,* 2011, vol. 13, no. 6, pp. 2497–2507. https://doi.org/10.1007/s11051-010-0143-8
29. Lin, H., Huang, C.P., Li, W., Ismat Shah, S., and Tseng, Y.-H., Size dependency of nano-crystalline TiO_2 on its optical property and photocatalytic reactiv-

ity exemplified by 2-chlorophenol, *Appl. Catal., B,* 2006, vol. 68, nos. 1–2, pp. 1–11. https://doi.org/10.1016/j.apcatb.2006.07.018

30. *Semiconductor Gas Sensors,* Jaaniso, R. and Kian Tan, O., Eds., Oxford: Woodhead Publ., 2013.
31. Gurlo, A. and Riedel, R., In situ and operando spectroscopy for assessing mechanisms of gas sensing, *Angew. Chem.,* 2007, vol. 46, pp. 3826–3848. https://doi.org/10.1002/anie.200602597
32. Chu, X., Dongli, J., and Chenmou, Z., The preparation and gas-sensing properties of $NiFe_2O_4$ nanocubes and nanorods, *Sens. Actuators, B,* 2007, vol. 123, no. 2, pp. 793–797. https://doi.org/10.1016/j.snb.2006.10.020
33. Sutka, A. and Gross, A., Spinel ferrite oxide semiconductor gas sensors, *Sens. Actuators, B,* 2016, vol. 222, pp. 95–105. https://doi.org/10.1016/j.snb.2015.08.027
34. Yang, L., Xie, Y., Zhao, H., Wu, X., and Wang, Y., Preparation and gas-sensing properties of $NiFe_2O_4$ semiconductor materials, *Solid-State Electron.,* 2005, vol. 49, no. 6, pp. 1029–1033. https://doi.org/10.1016/j.sse.2005.03.022
35. Choi, J., Byun, J., and Sub, S., Chemical influence of grain size on gas-sensing properties of chemiresistive *p*-type NiO nanofibers, *Sens. Actuators, B,* 2016, vol. 227, pp. 149–156. https://doi.org/10.1016/j.snb.2015.12.014
36. Kruefu, V., Wisitsoraat, A., Phokharatkul, D., Tuantranont, A., and Phanichphant, S., Chemical enhancement of *p*-type gas-sensing performances of NiO nanoparticles prepared by precipitation with RuO_2 impregnation, *Sens. Actuators, B,* 2016, vol. 236, no. 2, pp. 466–473. https://doi.org/10.1016/j.snb.2016.06.028

Translated by K. Lazarev